

中国激光

超音速激光沉积与激光熔覆 Stellite-6 涂层的抗气蚀性能及其机制对比研究

孙景勇^{1,2}, 晏宇亮^{1,2}, 李波^{1,2,3*}, 施其健^{1,2}, 徐天书⁴, 张群莉^{1,2}, 姚建华^{1,2}

¹ 浙江工业大学激光先进制造研究院, 浙江 杭州 310023;

² 浙江工业大学机械工程学院, 浙江 杭州 310023;

³ 江苏亚威机床股份有限公司, 江苏 扬州 225200;

⁴ 国网宁夏电力有限公司检修公司, 宁夏 银川 750011

摘要 利用超音速激光沉积(SLD)和激光熔覆(LC)两种基于激光的加工技术在 17-4 PH 不锈钢的表面上制备 Stellite-6 涂层, 并对涂层的微观特性以及气蚀机制进行分析。结果表明, LC 技术所制备的涂层在气蚀过程中表现出较大的累积失重量和气蚀速率, SLD 技术所制备的涂层则保持较小的气蚀速率。由于 SLD 技术的激光能量密度小于 LC 技术, 故 SLD 技术所制备的涂层保持原始粉末中细小的枝晶组织结构, 避免基体元素对涂层的稀释。对于 SLD 技术所制备的涂层, 由粉末颗粒塑性变形导致的加工硬化使其硬度与弹性模量的比高于 LC 技术所制备的涂层。上述因素均是 SLD 技术所制备涂层的抗气蚀性能优于 LC 技术所制备涂层的原因。

关键词 激光技术; 超音速激光沉积; 激光熔覆; Stellite-6 涂层; 气蚀

中图分类号 TN249; TG146.1

文献标志码 A

doi: 10.3788/CJL202148.1002118

1 引言

叶片作为工业汽轮机能量转换的核心部件之一, 对汽轮机的安全运行起着至关重要的作用。然而, 汽轮机的末级叶片在湿蒸汽腐蚀介质的环境中工作, 承受离心力、蒸汽作用力、激振力以及水滴冲刷的共同作用, 而且极易发生气蚀, 这会导致机组发生强烈振动和叶片断裂等恶性事件。由于气蚀通常自叶片表面开始, 因此利用涂层技术在叶片表面制备抗气蚀强化涂层是一种经济有效的方法, 而且已引起国内外学者的广泛关注^[1-5]。

目前, 研究较多的叶片抗气蚀涂层材料主要包括 Ni 基合金^[6]、Co 基合金^[6-7] 和 Fe 基合金^[8], 其中 Co 基合金(尤其是 Stellite-6 合金)因其具有良好的耐腐蚀、耐磨损以及耐高温的性能, 被广泛认为是汽轮机叶片抗气蚀涂层理想的材料之一^[9-12]。在抗气蚀涂层的制备工艺开发方面, 目前研究较多的是激

光熔覆(Laser Cladding, LC)、激光合金化、激光淬火等激光表面技术^[1] 以及热喷涂或冷喷涂等技术^[2,4-5,8]。激光熔覆和热喷涂涉及涂层/基体的高温熔化过程, 当热输入较大时, 使涂层存在相变、稀释和分解等热致不良影响, 影响涂层的抗气蚀性能; 激光合金化和激光淬火则主要存在表面改性层厚度有限的问题; 冷喷涂是一种基于材料塑性变形(不熔化)实现粉末颗粒沉积的方法^[13], 该方法虽然能够避免激光熔覆和热喷涂中存在的热致不良影响, 但对沉积材料的塑性变形能力具有一定的要求, 特别是在沉积高强度材料(如 Stellite-6)的过程中, 由于粉末颗粒的塑性变形能力有限, 则存在沉积效率低、涂层致密性差和界面结合弱等问题^[14]。因此, 抗气蚀涂层制备工艺的开发仍然是目前表面工程领域的研究热点之一。

超音速激光沉积(Supersonic Laser Deposition, SLD)是近年来发展起来的一种新型材料沉积方法,

收稿日期: 2020-10-28; 修回日期: 2020-11-17; 录用日期: 2020-12-14

基金项目: 国家自然科学基金(51701182, 52075495)、中国博士后科学基金(2020T130263, 2019M662103)

* E-mail: libo1011@zjut.edu.cn

其是一种将激光加热与冷喷涂同步耦合的激光复合制造技术^[15]。该技术在制备高强度材料以及热敏感复合材料涂层方面表现出独特的优势,已报道的材料包括 Ti6Al4V、diamond/Ni60、diamond/Cu、WC/SS316L 和 WC/Cu 等^[16-20]。此外,国内外学者利用 SLD 技术成功制备了 Stellite-6 涂层,并将其与 LC 技术所制备的 Stellite-6 涂层进行对比研究^[21-24]。研究结果表明,SLD 涂层技术所制备的涂层较 LC 涂层技术具有更优的耐磨损性能以及耐电化学腐蚀性能,但目前鲜有文献对 SLD 和 LC 两种技术所制备的 Stellite-6 涂层的抗气蚀性能进行对比研究。除了涂层材料以及制备工艺以外,国内外学者在抗气蚀涂层性能的影响因素方面也开展了大量的研究工作。目前普遍认为,抗气蚀涂层的性能与其微观结构、硬度、弹塑性、孔隙率、界面结合和稀释率等因素密切相关^[10,25-28]。由于 SLD 与 LC 两种技术沉积粉末材料的原理不同,因此这两种技术工艺所制备的 Stellite-6 涂层在微观特性(如组织结构、稀释率、界面结合和显微硬度等)方面会存在差异,而这些差异必然会对抗气蚀性能产生影响,目前鲜有文献报道该方面的工作,而且这两种技术工艺

所制备的涂层在气蚀机制方面的差异目前也不明晰。

因此,本文采用 SLD 和 LC 两种技术在 17-4 PH 不锈钢(叶片常用材料)基体的表面上制备 Stellite-6 涂层,并从微观组织、稀释率、弹性模量和硬度等角度对其抗气蚀性能进行评估,通过对气蚀形貌的分析,揭示两种涂层的气蚀机制。本文的研究工作有望为汽轮机叶片抗气蚀涂层的制备以及性能优化提供工艺支撑和理论指导。

2 实验材料和方法

2.1 实验材料

涂层所用的 Stellite-6 粉末为商业购买,显微形貌如图 1 所示,化学成分如表 1 所示。LC 和 SLD 两种技术工艺均采用球形粉末,LC 技术采用的粉末粒径范围为 50~100 μm,如图 1(a)所示;SLD 技术由于需要将粉末颗粒加速到超音速,因此采用粒径较小的粉末,粒径范围为 5~20 μm,如图 1(b)所示。基体材料选用 17-4 PH 不锈钢平板,化学成分如表 2 所示。基体尺寸为 120 mm × 60 mm × 17 mm,制备前采用 LC 技术和 SLD 技术对其进行去污和去脂处理,SLD 基板还需进行喷砂预处理。

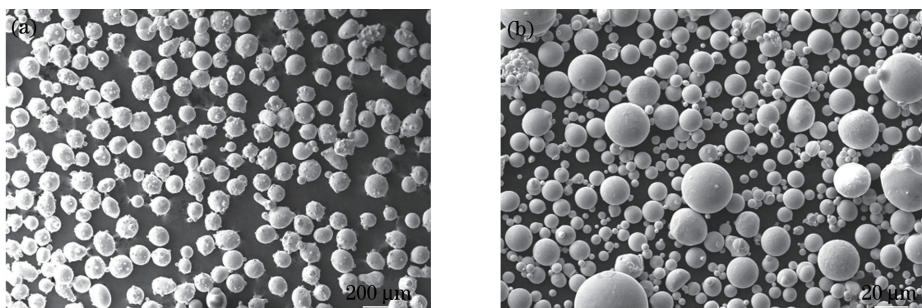


图 1 不同技术所需的 Stellite-6 粉末显微形貌。(a)LC 技术;(b)SLD 技术

Fig. 1 Micromorphology of Stellite-6 powder required by different technologies. (a) LC technology; (b) SLD technology

表 1 Stellite-6 粉末的化学成分

Table 1 Chemical composition of Stellite-6 powder

Element	Co	Cr	W	C	Ni	Mo	Fe	Si	Mn	Others
Mass fraction /%	Bal.	29.00	4.00	1.20	3.00	1.50	3.00	1.10	1.00	<1.0

表 2 17-4 PH 不锈钢基体的化学成分

Table 2 Chemical composition of 17-4 PH stainless steel substrate

Element	Fe	Cr	Ni	Cu	Si	Mn
Mass fraction /%	Bal.	17.00	4.00	4.00	1.00	1.00

2.2 实验系统与涂层制备

图 2 为实验所用的 SLD 系统,该系统主要由光纤耦合半导体激光器、冷喷涂设备、高压气瓶组和机

械臂组成。从高压气瓶组输出的氮气分两路进入冷喷涂设备中:一路进入送粉器中,另一路进入气体加热器中。送粉器中的高压气流携带喷涂粉末并与经

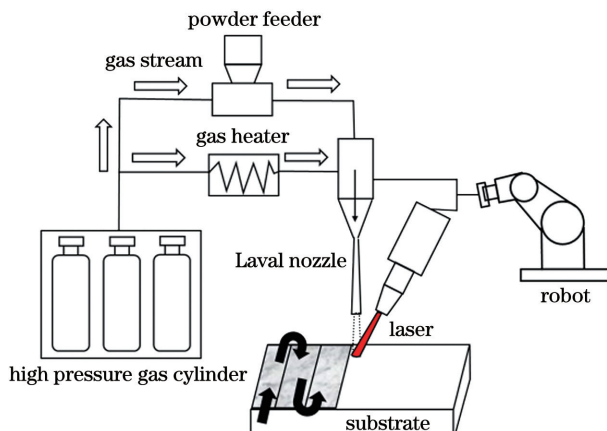


图 2 超音速激光沉积系统

Fig. 2 Supersonic laser deposition system

过气体加热器预热的气流在 Laval 喷嘴中进行混合加速, 加速后撞击激光同步加热的基体表面。在涂层制备过程中, Laval 喷嘴和激光头的运动轨迹由机械臂来控制, Laval 喷嘴加速后的粉末流垂直撞

击基板, 激光束与粉末流成 30° 夹角, 粉末流与激光束相互作用的关系如图 3 所示。粉末流与激光束在激光器的焦平面(焦距为 400 mm)上重合, 制备过程未采取离焦处理(离焦量为 0)。优化后的 SLD 系统制备 Stellite-6 涂层的工艺参数如表 3 所示。

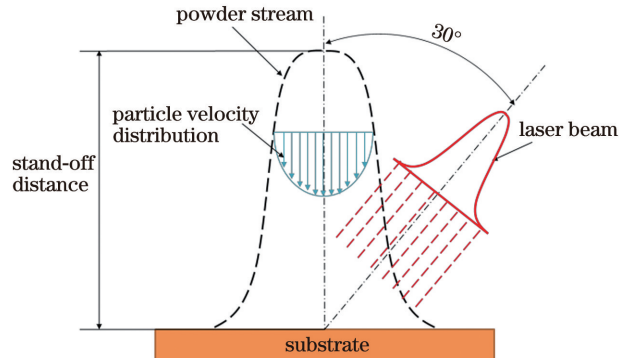


图 3 粉末流与激光束相互作用的关系

Fig. 3 Relationship between powder flow and laser beam interaction

表 3 SLD 制备 Stellite-6 涂层的工艺参数

Table 3 Process parameters of Stellite-6 coating prepared by SLD

Parameter	N_2 pressure / MPa	N_2 temperature / °C	Stand-off distance / mm	Powder feeding rate/ ($r \cdot min^{-1}$)	Traverse speed/ ($mm \cdot s^{-1}$)	Laser power / kW	Laser spot diameter/ mm	Overlapping rate/ %
Value	4	700	30	2.5	10	1.1	4	50

LC 技术采用与 SLD 技术相同的激光器, 以氩气作为载气和保护气, 送粉方式为沸腾式同轴送粉方式。LC 技术的制备过程与 SLD 技术相同, 制备

过程未采取离焦处理。优化后的 LC 系统制备 Stellite-6 涂层的工艺参数如表 4 所示。

表 4 LC 制备 Stellite-6 涂层的工艺参数

Table 4 Process parameters of Stellite-6 coating prepared by LC

Parameter	Laser power/ kW	Laser spot diameter/ mm	Traverse speed/ ($mm \cdot s^{-1}$)	Power feeding rate/ ($g \cdot min^{-1}$)	Overlapping rate/ %
Value	1.6	4	7	13	50

2.3 涂层结构与性能表征

涂层的抗气蚀性能根据标准 ASTM G32 采用超声气蚀的方法进行测试, 测试装置如图 4 所示, 加工后的气蚀试样实物如图 5 所示。气蚀试样与超声变幅杆的底部以螺纹连接的方式进行装配, 测试介质为质量分数为 3.5% 的 NaCl 溶液, 温度保持在 25 °C。测试过程中, 气蚀试样的涂层侧浸入介质溶液中 20 mm 处, 超声振动频率为 20 kHz, 峰-峰振幅为 50 μm。气蚀测试时长为 14 h, 试样每经过 1 h 气蚀后取出并使用乙醇清洗后吹干, 然后使用电子秤(精度为 0.001 mg)称重

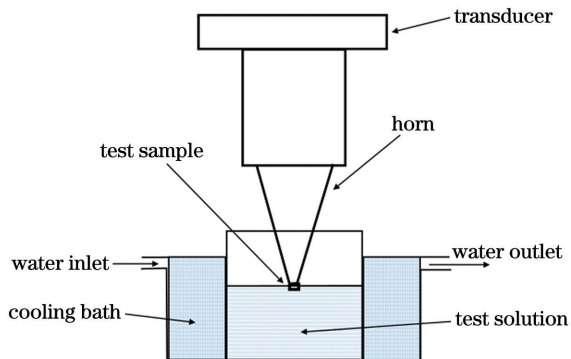


图 4 气蚀测试装置

Fig. 4 Cavitation test equipment

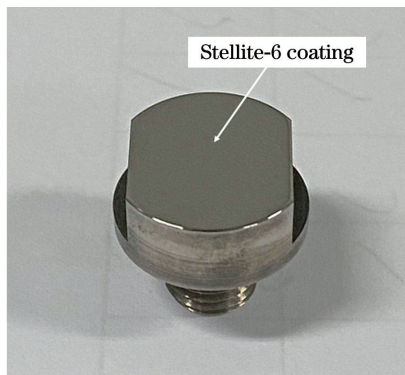


图5 气蚀试样实物

Fig. 5 Cavitation sample material

三次取平均值,记录失重量后继续实验。抗气蚀性能主要通过累积失重量和气蚀速率来表征,气蚀速率的表达式为

$$V_c = \frac{W_{t_2} - W_{t_1}}{t_2 - t_1}, \quad (1)$$

式中: V_c 为气蚀速率,单位为 mg/h; t_1 和 t_2 为气蚀时间,单位为 h; W_{t_1} 和 W_{t_2} 分别为气蚀 t_1 和 t_2 后的累积失重量,单位为 mg。

使用光学显微镜(OM)和扫描电子显微镜(SEM)来观察涂层的截面形貌和微观组织以及气蚀试样的表面形貌。使用能谱仪(EDS)来分析涂层/基体界面处的元素分布。使用维氏硬度计来测试涂层的显微硬度,测试载荷为 200 g,加载时间为 10 s,每次测试取 5 个测试点的平均值作为最终的显微硬度值。使用纳米压痕仪在室温条件下以连续刚度法(恒定应变速率 0.05 s^{-1})来测试涂层的弹性模量和硬度,每个试样测试 6 个点,取其平均值作为最终结果。

3 分析与讨论

3.1 涂层抗气蚀性能评估

表 5 为 LC 技术和 SLD 技术所制备的 Stellite-6 涂层的气蚀累积失重量以及气蚀速率随气蚀时间的变化情况。从表 5 可以看到,前 2 h 内,两种技术所制备的 Stellite-6 涂层具有相似的累积失重量和气蚀速率,这对应气蚀过程的孕育阶段,此阶段气蚀速率缓慢(小于 1 mg/h);在随后的阶段,LC 技术所制备试样的累积失重量快速增加,气蚀速率迅速增加并保持在 2 mg/h 以上,SLD 技术所制备试样的累积失重量缓慢增长,气蚀速率在整个气蚀过程中基本保持在 0.7 mg/h 左右,仅在气蚀时间为 14 h 时增至 1 mg/h 以上。

表 5 LC 技术和 SLD 技术所制备的 Stellite-6 涂层的气蚀累积失重量和气蚀速率对比

Table 5 Comparison of cavitation mass loss and cavitation rate of Stellite-6 coatings prepared by LC technology and SLD technology

Cavitation time/ h	Cumulative mass loss/ mg		Cavitation rate/ (mg•h ⁻¹)	
	LC	SLD	LC	SLD
1	0.76	0.80	0.76	0.80
2	1.73	1.57	0.97	0.77
3	4.20	2.13	2.47	0.56
4	7.12	2.89	2.92	0.76
5	10.15	3.64	3.03	0.75
6	12.92	4.18	2.77	0.54
7	15.87	4.82	2.95	0.64
8	18.66	5.43	2.79	0.61
9	21.35	6.16	2.69	0.73
10	24.02	6.88	2.67	0.72
11	26.57	7.60	2.65	0.72
12	29.46	8.37	2.79	0.77
13	32.16	9.18	2.70	0.81
14	34.82	10.23	2.66	1.05

图 6 为 LC 技术和 SLD 技术所制备的 Stellite-6 涂层在不同气蚀时间后的表面宏观形貌。从图 6 可以看到,LC 技术所制备的试样经过 1 h 气蚀后,试样表面的金属光泽几乎全部消失,试样表面的气蚀程度随着气蚀时间的延长不断加剧,SLD 技术所制备的试样在经过 1 h 的气蚀后,试样表面的金属光泽几乎不受影响,随着气蚀过程的继续进行,单道沉积层相搭接的部位(图 6 凹下去的部位)逐渐显现出来,表明这些区域首先被气蚀;当气蚀时间达到 7 h 时,单道沉积层内开始出现气蚀斑点,随着气蚀时间的延长,气蚀斑点不断扩散;当气蚀时间为 13 h 时,扩展的气蚀斑点相互连接形成一块面积较大的气蚀区域。综上,LC 技术和 SLD 技术所制备的 Stellite-6 试样气蚀后的表面形貌演变规律与表 5 的累积失重量和气蚀速率随时间的变化规律一致。此外,值得注意的是,SLD 技术所制备的试样即使经过 13 h 的气蚀测试,其气蚀程度仍比仅经过 3 h 气蚀测试的 LC 技术所制备的试样轻。表 5 和图 6 的结果均表明,SLD 技术所制备的试样比 LC 技术具有更优的抗气蚀性能。

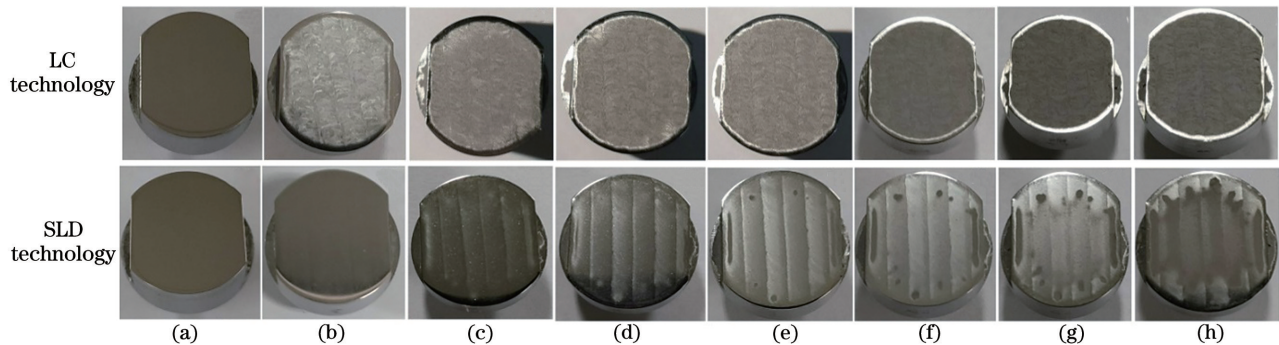


图 6 不同技术在不同气蚀时间下的 Stellite-6 涂层表面宏观形貌。(a) 0 h;(b) 1 h;(c) 3 h;(d) 5 h;(e) 7 h;(f) 9 h;
(g) 11 h;(h) 13 h

Fig. 6 Surface macroscopic morphology of Stellite-6 coating at different cavitation time by different technologies. (a) 0 h;
(b) 1 h;(c) 3 h; (d) 5 h; (e) 7 h; (f) 9 h; (g) 11 h; (h) 13 h

3.2 涂层微观特性表征

为了阐明 LC 技术和 SLD 技术所制备的 Stellite-6 涂层存在抗气蚀性能差异的原因,对两种技术所制备的涂层微观特性进行表征。图 7 为 LC 技术和 SLD 技术所制备的多道搭接 Stellite-6 涂层的横截面显微形貌。从图 7 可以看到,LC 技术所制备的涂层表面较为平整,涂层 /

基体界面结合处呈弧线状,而 SLD 技术所制备的涂层表面则出现起伏特征,涂层/基体界面结合处较为平整;在高倍扫描电镜下对形貌进行观察,LC 技术所制备的涂层呈现出典型的粗大熔覆枝晶结构,而 SLD 技术所制备的涂层保持了沉积粉末颗粒内部的细小枝晶结构,这与输入的激光能量有关。

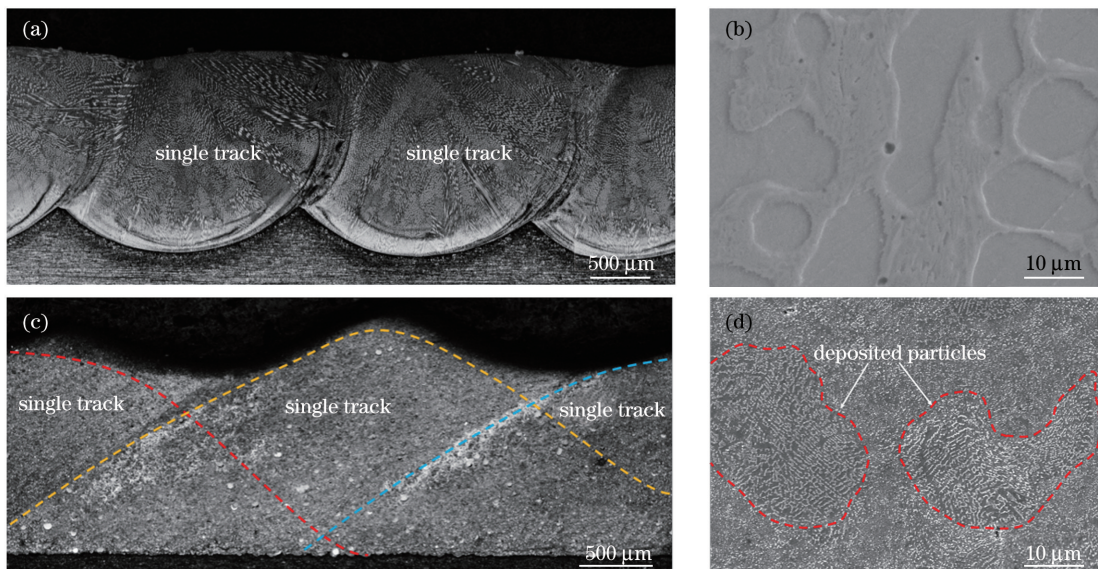


图 7 不同技术制备的 Stellite-6 多道搭接涂层的横截面形貌及高倍放大图。(a)(b)LC 技术;(c)(d)SLD 技术

Fig. 7 Cross-section morphology and high magnification of Stellite-6 multi-channel lap coating prepared by different technologies. (a) (b) LC technology; (c) (d) SLD technology

激光加工过程中,激光的功率密度(p)由输出功率(P)和光斑直径(d)决定,表达式

$$p = \frac{4P}{\pi d^2}。 \quad (2)$$

激光与基材的相互作用时间(t)由激光的扫描速度(v)和 d 确定,表达式为

$$t = \frac{d}{v}。 \quad (3)$$

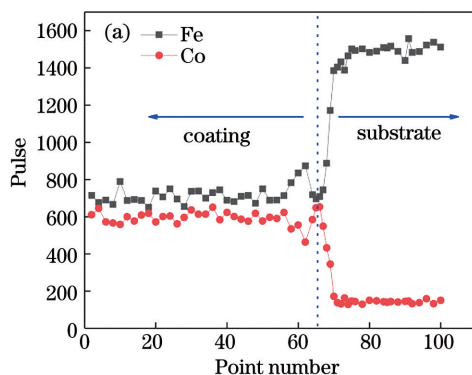
结合(2)式和(3)式可以计算基材表面的激光能量密度(e),表达式为

$$e = pt = \frac{4P}{\pi d v}。 \quad (4)$$

根据表 3 和表 4 的工艺参数,计算得到 LC 技术和 SLD 技术使用的激光能量密度分别为 $e_{SLD} = 35.03 \text{ J/mm}^2$ 和 $e_{LC} = 72.79 \text{ J/mm}^2$, e_{LC} 是 e_{SLD} 的 2 倍。LC 技术使用较高的激光能量密度会使基材

和沉积粉末熔化，在随后的凝固结晶过程中由于热输入大会使重新形成的枝晶相较于原始粉末中的枝晶有所长大，而 SLD 技术使用较低的激光能量密度，沉积粉末不熔化，这是一个固态沉积过程，因此仍然保持了原始粉末颗粒内部的细小枝晶结构。文献[29]报道了晶粒细化有利于提高材料的抗气蚀性能，因此 SLD 技术所制备的涂层中较细的枝晶结构是其抗气蚀性能优于 LC 技术所制备的涂层的一个重要原因。

图 8 是 LC 技术和 SLD 技术所制备的 Stellite-6 涂层与基体界面结合处的 Co 元素和 Fe 元素分布曲



线。由于涂层与基体中均含有 Cr、Ni、Si 和 Mn 等元素(表 1 和表 2)，因此只测试 Co 和 Fe 两种元素在涂层和基体中的分布以对比两种工艺的稀释率。从图 8 可以看到，在 LC 技术所制备的涂层中能够明显检测到来自基体的 Fe 元素，表明其稀释率较大，而 SLD 技术所制备的涂层中几乎检测不到 Fe 元素，说明该涂层几乎无稀释，这与其固态非熔化的沉积机制相关。基体中的 Fe 元素进入涂层中会改变 Stellite-6 合金的原始化学成分，从而影响其抗气蚀性能，LC 技术所制备涂层具有较高的稀释率，这是其抗气蚀性能不如 SLD 技术所制备涂层的原因之一。

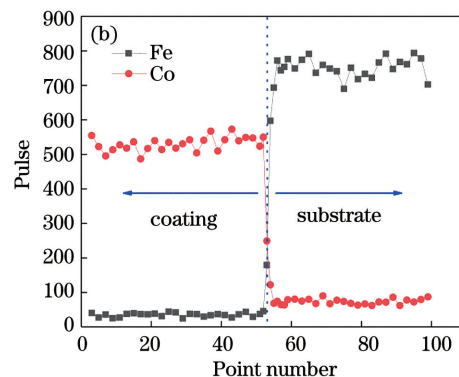


图 8 不同技术制备的 Stellite-6 涂层/基体界面的元素分析。(a) LC 技术；(b) SLD 技术

Fig. 8 Elemental analysis of Stellite-6 coating/substrate interface prepared by different technologies. (a) LC technology; (b) SLD technology

图 9 为 LC 技术和 SLD 技术所制备的 Stellite-6 涂层的纳米压痕测试结果。从图 9 可以看到，SLD 技术所制备涂层的弹性模量为 (206.1 ± 8.4) GPa，硬度为 (8.64 ± 0.63) GPa，LC 技术所制备涂层的弹性模量为 (194.3 ± 26.6) GPa，硬度为 (5.42 ± 1.33) GPa。SLD 技术是基于材料塑性变形实现沉积的一种技术，涂层制备过程中，材料会出现加工硬化的现象，因此其硬度会比 LC 技术所制

备的涂层高。此外，有文献报道晶粒细化会提高材料的硬度^[30]，因此 SLD 技术所制备的涂层中较细的微观组织结构(图 7)也是其硬度较高的一个原因。根据文献[31]报道可知，高的硬度(H)和弹性模量(E)的比值(H/E)代表涂层对气蚀气泡反复冲击所产生的弹性变形功具有更高的吸收能力，即具有更好的抗气蚀性能。根据图 9 的结果计算可得，SLD 技术所制备涂层的 H/E 值为 0.042，而

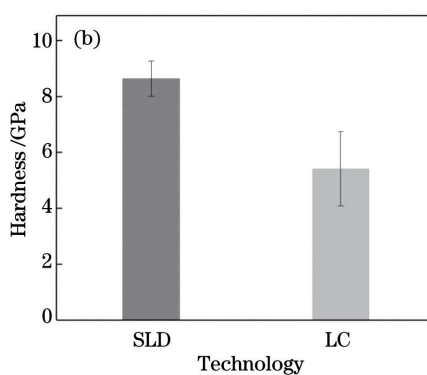
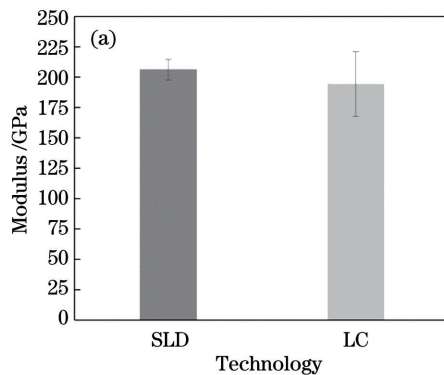


图 9 LC 技术和 SLD 技术所制备的 Stellite-6 涂层的纳米压痕测试结果。(a) 弹性模量；(b) 硬度

Fig. 9 Nanoindentation test results of Stellite-6 coating prepared by LC technology and SLD technology. (a) Modulus of elasticity; (b) hardness

LC 技术所制备涂层的 H/E 值为 0.028。因此, SLD 技术所制备涂层较高的 H/E 值也是其抗气蚀性能优于 LC 技术所制备涂层的一个原因。

3.3 涂层气蚀机制分析

为了对比研究 LC 技术和 SLD 技术所制备的 Stellite-6 涂层的气蚀机制, 对经过不同气蚀时间后的涂层表面显微形貌进行分析。图 10 为 LC 技术所制备的涂层经过 7 h 和 13 h 气蚀后的表面显微形貌。从图 10 可以看到, 经过 7 h 和 13 h 气蚀后

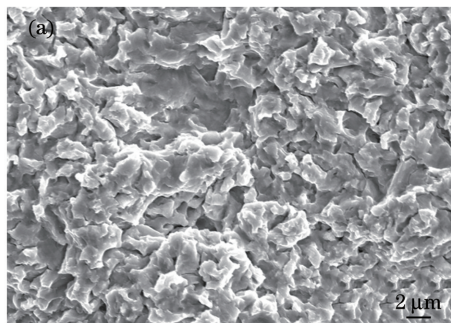


图 10 LC 技术所制备的 Stellite-6 涂层在不同气蚀时间后的表面显微形貌。(a) 7 h;

Fig. 10 Surface morphology of Stellite-6 coating prepared by LC technology after different cavitation time.

(a) 7 h; (b) 13 h

图 11 为 SLD 技术所制备的涂层经过 7 h 和 13 h 气蚀后的表面显微形貌。从图 11(a)可以看到, 经过 7 h 的气蚀测试后, SLD 技术所制备涂层的表面出现了许多尺寸在 $5\sim30 \mu\text{m}$ 之间的气蚀小坑, 呈现出一种非均匀气蚀的表面形貌, 这与图 10(a)LC 技术所制备的涂层经过 7 h 气蚀后的试样形貌完全不同。如前所述, SLD 技术是一种基于材料塑性变形实现沉积的过程, 粉末颗粒与颗粒之间的结合机制主要为机械结合, 而非 LC 技术的

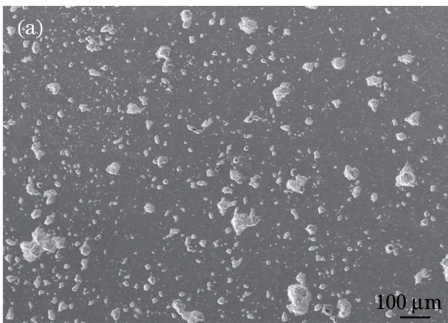


图 11 SLD 技术所制备的 Stellite-6 涂层在不同气蚀时间后的表面显微形貌。(a) 7 h;

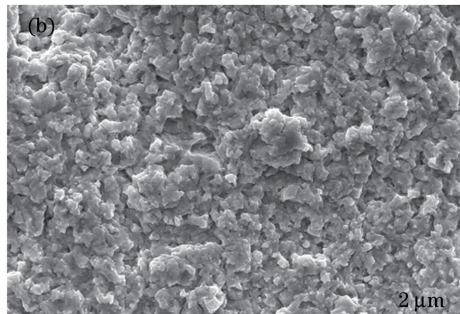
Fig. 11 Surface morphology of Stellite-6 coating prepared by SLD technology after different cavitation time. (a) 7 h;

(b) 13 h

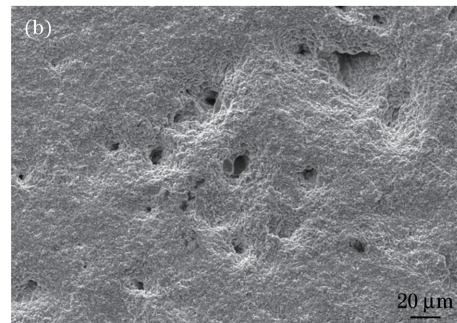
4 结 论

对比研究 LC 技术和 SLD 技术所制备的

的表面形貌基本相同, 呈现出一种均匀气蚀的过程, 与文献[10]报道的激光熔覆 Stellite-6 涂层的气蚀形貌一致。LC 技术所制备的涂层是基于材料熔化/凝固冶金过程形成的, 微观组织是典型的枝晶结构, 存在许多的晶界/相界。晶界/相界是材料中的薄弱环节, 这些位置在气蚀过程中会优先产生微孔隙/裂纹并在气泡不断冲击破裂的过程中逐渐扩展, 最终导致材料损坏^[32], 形成的气蚀形貌如图 10 所示。



冶金结合, 因此在粉末沉积的过程中存在颗粒间结合不良所导致的孔隙, 如图 12 所示。这些孔隙会成为产生气泡的优先位置^[33], 在随后气泡破灭的冲击作用下, 孔隙周围结合不良的颗粒就会从涂层中掉落下来, 形成气蚀坑。这些气蚀坑又成为后续气蚀的优先位置, 在这些位置处会产生微裂纹并沿晶界/相界等位置不断扩展(与 LC 技术所制备涂层的气蚀过程类似)直至相互连接形成较大的气蚀区域(材料脱落), 从而呈现的气蚀形貌如图 11(b)所示。



Stellite-6 涂层的抗气蚀性能, 并从微观特性的角度阐明两种涂层抗气蚀性能优劣的原因, 通过对气蚀表面形貌进行分析来对比研究两种涂层气蚀机制的

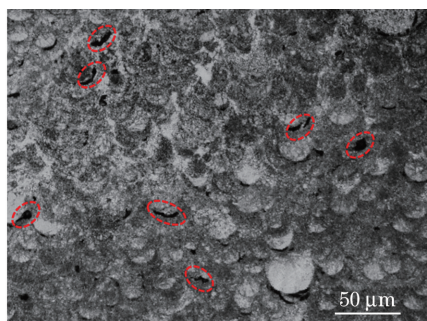


图 12 SLD 技术所制备的 Stellite-6 涂层的孔隙情况

Fig. 12 Porosity of Stellite-6 coating prepared by SLD technology

差异。实验结果表明,LC 技术所制备的涂层在经过 2 h 的气蚀孕育期后,累计失重量迅速增加,气蚀速率维持在 2 mg/h 以上,试样表面呈现较为严重的气蚀特征;SLD 技术所制备的涂层在整个气蚀测试过程中均维持较低的累积失重量,气蚀速率稳定在 0.7 mg/h 左右,表明 SLD 技术所制备的涂层较 LC 技术所制备的涂层具有更优的抗气蚀性能。在较低的激光输入能量密度的情况下,SLD 技术所制备的涂层较 LC 技术所制备的涂层具有更细小的枝晶结构和更低的元素稀释率。此外,SLD 技术是基于材料塑性变形实现粉末颗粒沉积的过程,这会出现加工硬化的现象,因此 SLD 技术所制备的涂层较 LC 技术所制备的涂层具有更高的硬度/弹性模量比。这些因素将会导致 SLD 技术所制备的涂层较 LC 技术所制备的涂层具有更好的抗气蚀性能。LC 技术是基于材料熔化/凝固冶金过程形成的,具有典型的枝晶组织结构,相界/晶界部分是气蚀优先发生的位置,为此呈现出均匀气蚀的表面形貌,而 SLD 技术所制备的涂层是依靠机械结合而非冶金结合来实现材料沉积,所以颗粒间会存在结合不良导致的孔隙,这些位置是气蚀发生的优先位置,为此呈现出一种非均匀气蚀的过程。

参 考 文 献

- [1] Kwok C T, Man H C, Cheng F T, et al. Developments in laser-based surface engineering processes: with particular reference to protection against cavitation erosion[J]. Surface and Coatings Technology, 2016, 291: 189-204.
- [2] Du J, Zhang J F, Xu J Y, et al. Cavitation-corrosion behaviors of HVOF sprayed WC-25WB-10Co-5NiCr and MoB-25NiCr coatings[J]. Ceramics International, 2020, 46(13): 21707-21718.
- [3] Ma D N, Harvey T J, Zhuk Y N, et al. Cavitation erosion performance of CVD W/WC coatings [J]. Wear, 2020, 452: 203276.
- [4] Szala M, Latka L, Walczak M, et al. Comparative study on the cavitation erosion and sliding wear of cold-sprayed Al/Al₂O₃ and Cu/Al₂O₃ coatings, and stainless steel, aluminium alloy, copper and brass [J]. Metals, 2020, 10(7): 856.
- [5] Kazasidis M, Yin S, Cassidy J, et al. Microstructure and cavitation erosion performance of nickel-Inconel 718 composite coatings produced with cold spray[J]. Surface and Coatings Technology, 2020, 382: 125195.
- [6] Sreedhar B K, Albert S K, Pandit A B. Improving cavitation erosion resistance of austenitic stainless steel in liquid sodium by hardfacing-comparison of Ni and Co based deposits[J]. Wear, 2015, 342/343: 92-99.
- [7] Hou G L, Ren Y, Zhang X L, et al. Cavitation erosion mechanisms in Co-based coatings exposed to seawater[J]. Ultrasonics Sonochemistry, 2020, 60: 104799.
- [8] Silveira L L, Pukasiewicz A G M, de Aguiar D J M, et al. Study of the corrosion and cavitation resistance of HVOF and HVAF FeCrMnSiNi and FeCrMnSiB coatings [J]. Surface and Coatings Technology, 2019, 374: 910-922.
- [9] Cui C, Wu M P, Cheng W. Effect of laser power on corrosion resistance of 42CrMo cladding Stellite-6 coating [J]. Laser & Optoelectronics Progress, 2019, 56(24): 241403.
- [10] Singh R, Kumar D, Mishra S K, et al. Laser cladding of Stellite 6 on stainless steel to enhance solid particle erosion and cavitation resistance [J]. Surface and Coatings Technology, 2014, 251: 87-97.
- [11] Yu T, Zhang Z X, Rao X X, et al. High-temperature wear behavior of laser-cladding Stellite 6 coating [J]. Laser & Optoelectronics Progress, 2019, 56 (14): 141403.
- [12] Cui C, Wu M P, Xia S H. Effect of heat treatment on properties of laser cladding cobalt-based coating on 42CrMo steel surface[J]. Chinese Journal of Lasers, 2020, 47(6): 0602011.
- [13] 崔宸, 武美萍, 夏思海. 热处理对 42CrMo 钢表面激光熔覆钴基涂层性能的影响 [J]. 中国激光, 2020, 47(6): 0602011.

- [13] Li W Y, Yang K, Yin S, et al. Solid-state additive manufacturing and repairing by cold spraying: a review [J]. *Journal of Materials Science & Technology*, 2018, 34(3): 440-457.
- [14] Cinca N, López E, Dosta S, et al. Study of Stellite-6 deposition by cold gas spraying [J]. *Surface and Coatings Technology*, 2013, 232: 891-898.
- [15] Yao J H, Wu L J, Li B, et al. Research states and development tendency of supersonic laser deposition technology [J]. *Chinese Journal of Lasers*, 2019, 46(3): 0300001.
姚建华, 吴丽娟, 李波, 等. 超音速激光沉积技术: 研究现状及发展趋势 [J]. 中国激光, 2019, 46(3): 0300001.
- [16] Li B, Wu L J, Zhang X, et al. Microstructure and corrosion-resistant property of Ti6Al4V coating prepared by supersonic laser deposition [J]. *China Surface Engineering*, 2018, 31(5): 159-166.
李波, 吴丽娟, 张欣, 等. 超音速激光沉积 Ti6Al4V 涂层的微观结构及耐蚀性能 [J]. 中国表面工程, 2018, 31(5): 159-166.
- [17] Yao J H, Yang L J, Li B, et al. Beneficial effects of laser irradiation on the deposition process of diamond/Ni60 composite coating with cold spray [J]. *Applied Surface Science*, 2015, 330: 300-308.
- [18] Wu L J, Wang W L, Li B, et al. Influence of diamond particle size and content on the microstructure and properties of diamond/Cu composite coating prepared by supersonic laser deposition [J]. *Surface Technology*, 2019, 48(2): 40-46.
吴丽娟, 汪伟林, 李波, 等. 金刚石粒径及含量对超音速激光沉积金刚石/Cu 复合涂层微观结构及性能的影响 [J]. 表面技术, 2019, 48(2): 40-46.
- [19] Jin Y, Li B, Zhang X, et al. Deposition behavior and electrochemical failure mechanism of WC/SS316L metal matrix composites prepared by supersonic laser deposition [J]. *Chines Journal of Lasers*, 2018, 45(1): 0102001.
金琰, 李波, 张欣, 等. 金属基复合材料 WC/SS316L 超音速激光沉积行为及电化学失效机理 [J]. 中国激光, 2018, 45(1): 0102001.
- [20] Huang X J, Wu L J, Li B, et al. Microstructure characterization and tribological properties evaluation on WC/Cu composite coating prepared by supersonic laser deposition [J]. *Journal of Mechanical Engineering*, 2020, 56(10): 78-85.
黄煊杰, 吴丽娟, 李波, 等. 超音速激光沉积 WC/Cu 复合涂层的微观结构及耐磨性能表征 [J]. 机械工程学报, 2020, 56(10): 78-85.
- [21] Li Z H, Yang L J, Zhang Q L, et al. Comparative research of Stellite6 coatings prepared by supersonic laser deposition and laser cladding [J]. *Chinese Journal of Lasers*, 2015, 42(5): 0503008.
李祉宏, 杨理京, 张群莉, 等. 超音速激光沉积与激光熔覆 Stellite6 涂层的对比研究 [J]. 中国激光, 2015, 42(5): 0503008.
- [22] Lupoi R, Cockburn A, Bryan C, et al. Hardfacing steel with nanostructured coatings of Stellite-6 by supersonic laser deposition [J]. *Light: Science & Applications*, 2012, 1(5): e10.
- [23] Luo F, Cockburn A, Lupoi R, et al. Performance comparison of Stellite 6® deposited on steel using supersonic laser deposition and laser cladding [J]. *Surface and Coatings Technology*, 2012, 212: 119-127.
- [24] Luo F, Lupoi R, Cockburn A, et al. Characteristics of Stellite 6 deposited by supersonic laser deposition under optimized parameters [J]. *Journal of Iron and Steel Research, International*, 2013, 20(2): 52-57.
- [25] Deng W, Zhao X Q, Ren Y, et al. Influence of epoxy resin on the microstructure and cavitation erosion of as-sprayed 8YSZ coating [J]. *Ceramics International*, 2019, 45(5): 5693-5702.
- [26] Babu A, Arora H S, Singh H, et al. Microwave synthesized composite claddings with enhanced cavitation erosion resistance [J]. *Wear*, 2019, 422/423: 242-251.
- [27] Deng W, An Y L, Hou G L, et al. Effect of substrate preheating treatment on the microstructure and ultrasonic cavitation erosion behavior of plasma-sprayed YSZ coatings [J]. *Ultrasonics Sonochemistry*, 2018, 46: 1-9.
- [28] Ding X, Ke D, Yuan C Q, et al. Microstructure and cavitation erosion resistance of HVOF deposited WC-Co coatings with different sized WC [J]. *Coatings*, 2018, 8(9): 307.
- [29] Di Schino A, Salvatori I, Kenny J M. The effect of grain size on the mechanical and cavitation resistance of a high nitrogen and low nickel austenitic stainless steel [J]. *Materials Science Forum*, 2003, 426/427/428/429/430/431/432: 975-980.
- [30] Qin W B, Li J S, Liu Y Y, et al. Effects of grain size on tensile property and fracture morphology of 316L stainless steel [J]. *Materials Letters*, 2019, 254: 116-119.
- [31] Nair R B, Arora H S, Grewal H S. Microwave synthesized complex concentrated alloy coatings: plausible solution to cavitation induced erosion-corrosion [J]. *Ultrasonics Sonochemistry*, 2019, 50: 114-125.

- [32] Xu J, Zhang S K, Lu X L, et al. Effect of Al alloying on cavitation erosion behavior of TaSi₂ nanocrystalline coatings [J]. Ultrasonics Sonochemistry, 2019, 59: 104742.
- [33] Deng W, Hou G L, Li S J, et al. A new methodology to prepare ceramic-organic composite coatings with good cavitation erosion resistance [J]. Ultrasonics Sonochemistry, 2018, 44: 115-119.

Comparative Study on Cavitation-Resistance and Mechanism of Stellite-6 Coatings Prepared with Supersonic Laser Deposition and Laser Cladding

Sun Jingyong^{1,2}, Yan Yuliang^{1,2}, Li Bo^{1,2,3*}, Shi Qijian^{1,2}, Xu Tianshu⁴,
Zhang Qunli^{1,2}, Yao Jianhua^{1,2}

¹ Institute of Laser Advanced Manufacturing, Zhejiang University of Technology, Hangzhou, Zhejiang 310023, China;

² College of Mechanical Engineering, Zhejiang University of Technology, Hangzhou, Zhejiang 310023, China;

³ Jiangsu Yawei Machine Tool Co., Ltd., Yangzhou, Jiangsu 225200, China;

⁴ State Grid Ningxia Maintenance Company, Yinchuan, Ningxia 750011, China

Abstract

Objective As the core part of energy conversion of industrial steam turbine, the blade plays an important role in the safe operation of a steam turbine. However, the last stage blade usually suffers from cavitation, leading to severe vibration, blade fracture, and other malignant events. Since cavitation usually starts from the blade surface, it is an economic and effective method to prepare anti-cavitation coating on the blade surface by coating technology, which has attracted significant attention. Cobalt-based alloy Stellite-6 is widely considered as one of the most ideal materials for cavitation-resistant coating of steam turbine blades due to its good corrosion resistance, wear resistance, and high-temperature resistance. Traditional coating technologies, such as laser cladding (LC) and thermal spraying, have adverse thermally-induced effects, such as phase transformation, dilution, and decomposition. Supersonic laser deposition (SLD) technology is a material deposition technology combining laser and cold spraying. It can realize the deposition of high-strength materials (e.g., Stellite-6) while avoiding the adverse effects caused by massive heat input. In this study, SLD and LC are employed to prepare Stellite-6 coating. The cavitation-resistant properties of the two kinds of Stellite-6 coatings are evaluated. The underlying mechanisms are clarified based on microstructure, dilution ratio, elastic modulus, and hardness. This study is expected to provide process support and theoretical guidance for the fabrication and performance optimization of cavitation-resistant coating for steam turbine blades.

Methods Stellite-6 coating is prepared on 17-4 PH stainless steel through SLD and LC processes. The cavitation-resistant properties of the two kinds of coatings are tested using an ultrasonic cavitation method according to ASTM G32. The cavitation sample is assembled with the bottom of the ultrasonic horn through a thread connection. The test medium is NaCl (the mass fraction is 3.5%) solution and the constant temperature is 25 °C. During the test, the coating side of the cavitation sample is immersed in the medium solution for 20 mm, the ultrasonic vibration frequency is 20 kHz, and the peak-peak amplitude is 50 μm. The duration of the cavitation test is 14 h. After every 1 h of cavitation, the sample is taken out, cleaned with alcohol, and dried. Then, the sample is weighed with an electronic scale (accuracy of 0.001 mg) three times to take the average value. Mass loss is recorded before continuing the experiment. The cavitation-resistance is characterized by cavitation mass loss and cavitation rate.

Results and Discussions As shown in Table 1, in the first 2 h, Stellite-6 coatings prepared by LC and SLD processes have similar cavitation mass loss and cavitation rate, which corresponds to the incubation stage of the cavitation process, and the cavitation rate is slow (less than 1 mg/h). In the following stage, the cavitation mass loss of the LC sample increased rapidly, and the cavitation rate increased rapidly and remained above 2 mg/h. However, the cavitation mass loss of SLD sample increased slowly, and the cavitation rate remained at about 0.7 mg/h during the whole cavitation process and increased to more than 1 mg/h only when the cavitation time is 14 h.

The LC coating has a typical coarse cladding dendrite structure (Fig. 7 (b)), while the SLD coating retained the

fine dendrite structure inside the deposited powder particles (Fig. 7 (d)), which is related to the laser energy input during the two processes. The laser energy density is calculated to be 72.79 J/mm^2 and 35.03 J/mm^2 for LC and SLD processes, respectively. The fine dendrite structure of the original powder particles remained in the SLD coating due to lower heat input. It is reported that grain refinement is essential for improving the cavitation-resistance of materials. Thus, the finer dendrite structure in SLD coating is responsible for its better cavitation-resistance than LC coating.

As shown in Fig. 8 (a), the LC coating had severe element dilution of Fe from the substrate while Fe element is almost not detected in SLD coating (Fig. 8 (b)). The Fe element from the substrate changes the original chemical composition of the Stellite-6 alloy and affects its cavitation-resistance. The higher dilution degree of the LC coating is responsible for its inferior cavitation-resistance compared to that of the SLD coating. SLD is a material deposition process based on plastic deformation of powder and substrate. During the coating preparation process, the material will undergo work-hardening; thus, its hardness is higher than that of LC coating (Fig. 9), which is essential for cavitation-resistance.

To investigate the cavitation mechanism of the Stellite-6 coating prepared through LC and SLD, the surface morphology of the coating after different cavitation time is analyzed. The phase/grain boundary is the preferred position of cavitation in the LC coating, indicating a uniform surface morphology (Fig. 10). The pores between particles are the initial position of cavitation in the SLD coating, indicating a non-uniform cavitation process (Fig. 11).

Conclusions In this study, the cavitation-resistant properties of Stellite-6 coatings prepared by SLD and LC processes are compared. The reasons for the advantages and disadvantages of the two coatings are clarified from the perspective of micro characteristics. Through the analysis of cavitation surface morphology, the differences in cavitation mechanism between the two coatings are elucidated.

Due to the lower laser input energy density in the SLD process, the SLD coating has a finer dendrite structure and a lower element dilution ratio than the LC coating. Besides, SLD is a powder deposition process based on material plastic deformation, which induces a work-hardening effect. Thus, SLD coating has a higher hardness/elastic modulus ratio than LC coating. These factors lead to better cavitation-resistance of SLD coating than LC coating.

LC coating is formed through the material melting/re-solidification process, resulting in a typical dendrite structure. The phase/grain boundary is the preferred position of cavitation in the LC coating, which shows a uniform surface morphology. Since SLD relies on mechanical bonding instead of metallurgical bonding to fabricate coatings, there will be pores between particles due to poor bonding. These pores are the initial position of cavitation in SLD coating, showing a non-uniform cavitation process.

Key words laser technique; supersonic laser deposition; laser cladding; Stellite-6 coating; cavitation

OCIS codes 140.3390; 160.3900; 350.3390; 350.3850